Agriculture, Ecosystems and Environment 129 (2009) 391–400

Contents lists available at ScienceDirect

Agriculture, Ecosystems and Environment

journal homepage: www.elsevier.com/locate/agee

Modeling gross primary productivity for winter wheat–maize double cropping system using MODIS time series and CO_2 eddy flux tower data

Huimin Yan [a,*], Yuling Fu [a], Xiangming Xiao [b], He Qing Huang [a], Honglin He [a], Laura Ediger [a]

[a] Institute of Geographic Science and Natural Resources Research, Chinese Academy of Sciences, No. 11A, Datun Road, Anwai, Beijing 100101, China
[b] Institute for the Study of Earth, Oceans and Space, University of New Hampshire, Durham, NH 03824, USA

ARTICLE INFO

Article history:
Received 19 June 2008
Received in revised form 16 October 2008
Accepted 17 October 2008
Available online 5 December 2008

Keywords:
Crop intensity
Vegetation index
Vegetation photosynthesis model
Multiple cropping

ABSTRACT

Accurate and spatially explicit monitoring of gross primary productivity of agricultural ecosystems at a large scale is of great significance to assessment of crop conditions and agricultural production, and is necessary for understanding the carbon balance of the terrestrial biosphere. Identifying crop intensity (including multiple cropping and crop calendar) dynamics and assigning appropriate light use efficiency to C3 and C4 crops could substantially improve our ability to model and evaluate the seasonal dynamics of carbon flux in intensified agricultural ecosystems. In this paper, we have analyzed temporal dynamics of vegetation indices and phenological characteristics in the winter-wheat and maize double cropping system using multi-year satellite images from the moderate resolution imaging spectral radiometer (MODIS) and in situ observation of key crop phenological transition dates. The multiple cropping and crop calendar information were incorporated into simulations of the satellite-based vegetation photosynthesis model (VPM). Canopy-level maximum light use efficiency, a key parameter in the satellite-based VPM model, was estimated for both winter wheat (C3) and maize (C4) based on the observed CO_2 flux data from an eddy flux tower site in a winter wheat-maize double cropping agro-ecosystem in the Huang-Huai-Hai plain, China. The seasonal dynamics of GPP predicted by the VPM model agreed well with estimated GPP from eddy flux tower data. These results demonstrate the potential of the satellite-driven VPM model for scaling-up GPP estimation of intensified agricultural ecosystems, which is relevant to food production and security.

1. Introduction

Monitoring spatial and temporal variation in the amount of carbon dioxide fixed by crops is a central goal of ecosystem science. Gross primary production (GPP) is the first component of the carbon cycle, and is significant to understanding the global carbon cycle and evaluating effects of climate variation or crop management on food production (Running et al., 2004; Tao et al., 2005). In agricultural ecosystems, the physical characteristics of the cropping system change over time in response to localized and seasonal changes in climate, water resources and socio-economic conditions. Crop intensity, defined as the number of crops cultivated in a year in a particular field, is a key land management factor which is significant to the agricultural ecosystem carbon cycle, but has still not been accounted for in most ecosystem productivity or biogeochemical models (Bricklemyer et al., 2007; Zhang et al., 2008). Spatially explicit multiple cropping features remain a major source of uncertainty in the assessment of consequences of land use on food security and climate change (Li et al., 2003; Qiu et al., 2003).

Multiple cropping is the most intensive activity in an agro-ecosystem, and occurs in nearly 50% of China's cropland. Double-cropping in the Huang-Huai-Hai plain has been particularly important for ensuring China's food security over the past several decades (Qiu et al., 2003). The multiple cropping pattern can be measured in accordance with the phenological and ecological characteristics of crop growth by identifying the times of cropping cycles from time series of AVHRR/NDVI cloud-free composite images at 10-day intervals (Xin et al., 2002; Yan et al., 2005). Moderate resolution imaging spectroradiometer (MODIS) observation data with higher spatial resolution (500 m) and slightly shorter temporal frequency (8-day) is an even better option for accurate mapping of multiple-cropping.

MODIS time series image data holds considerable potential for advancing our capacity to estimate and monitor the biophysical characteristics and phenological changes of vegetation across large

* Corresponding author. Tel.: +86 10 6488 9467; fax: +86 10 6488 8992.
E-mail address: yanhm@igsnrr.ac.cn (H. Yan).

0167-8809/$ – see front matter © 2008 Elsevier B.V. All rights reserved.
doi:10.1016/j.agee.2008.10.017

geographic areas (Sakamoto et al., 2006; Zhang et al., 2006). MODIS vegetation indices (such as NDVI, EVI and LSWI) have been proved effective for quantifying vegetation greenness, canopy water content and crop intensity (Xiao et al., 2005b, 2006). The MODIS-based light use efficiency (LUE) models have been effectively used for continuous and rapid monitoring of national to global scale gross primary production from satellite-borne sensors, and the MODIS Land Science Team produces a standard data product for gross and net primary production of the world (MOD17) (Running et al., 1999). The results from a previous study (Zhang et al., 2008) showed that cropland GPP was underestimated in the GPP product (MOD17) when comparing the MODIS GPP product (MOD17) with estimated GPP from CO_2 eddy covariance flux measurements over a winter wheat and maize double-cropping field on the North China Plain; the mean annual GPP from MOD17 only accounted for about 1/5 to 1/3 of the flux tower-estimated GPP. Previous studies (Gower et al., 1999; Lobell et al., 2002; Bradford et al., 2005) indicated that differences among crop types in carboxylation biochemistry – notably, the C3 and C4 pathways – suggest associated differences in production efficiency (ε) which is linked to photosynthetic potential. Large areas of land surface are spatial and temporal mosaics of C3 and C4 photosynthetic types (Still et al., 2003), and crop type can change over time, even within a 1-year period, in the case of a rotation of C3 and C4 crops during a single year (e.g., winter wheat and maize). Because C4 plants have a more efficient photosynthetic capacity than C3 plants, assignment of one ε value across an entire year is problematic. The underestimation of GPP by the MOD17 data product further highlights the necessity of accounting for multiple cropping, especially with C3 and C4 crop rotation, in light use efficiency models for improving the accuracy of GPP estimation (Zhang et al., 2008).

Information about maximum light use efficiency for individual vegetation types can be obtained from analysis of net ecosystem exchange (NEE) of CO_2 and incident PAR (μmol/(m^2 s), photosynthetic photon flux density) at CO_2 eddy flux tower sites (Turner et al., 2003). GPP can also be estimated from CO_2 eddy flux tower data, which provides valuable information on seasonal dynamics of GPP for identifying the mechanism of LUE dynamics over different phenological stages (Wofsy et al., 1993; Soegaard et al., 2003).

Xiao et al. (2004a,b, 2005a,b) have developed a satellite-based vegetation photosynthesis model (VPM) that estimates the GPP of terrestrial ecosystems. The VPM model has been successfully used to estimate GPP using data from forest CO_2 flux tower sites (temperate deciduous broadleaf forest, evergreen coniferous forest, seasonally moist tropical forest) and grassland flux tower sites (Xiao et al., 2004a,b, 2005a,b; Li et al., 2007), but it is still unclear whether the VPM model can be used to estimate the GPP of managed croplands.

In this study, our objective is: (1) to characterize seasonal dynamics of winter wheat and maize from the MODIS vegetation indices; (2) to examine biophysical performance of vegetation indices in relation to seasonal dynamics of CO_2 fluxes; and (3) to evaluate the potential of the VPM model for estimating GPP of agricultural ecosystems with winter wheat–maize double cropping.

2. Study site and GPP estimation from eddy flux measurements

2.1. Description of study site

The Yucheng CO_2 flux station (36°57′N, 116°36′E) is located on the Huang-Huai-Hai plain, one of China's major food-producing regions. Double cropping of winter wheat and maize is the most popular cropping system in the Huang-Huai-Hai plain, accounting for more than 70% of total cropland land area (Fig. 1). This area is in a warm temperate zone and the climate is semi-humid monsoon. Mean annual global solar radiation at the Yucheng station is 5225 MJ/m^2, mean annual temperature is 13.1 °C and mean annual precipitation is 528 mm. Mean annual accumulated temperature of >0 °C is 4951 °C, and >10 °C is 4441 °C, with mean annual sunshine duration of 2640 h and a frost-free period of 200 days.

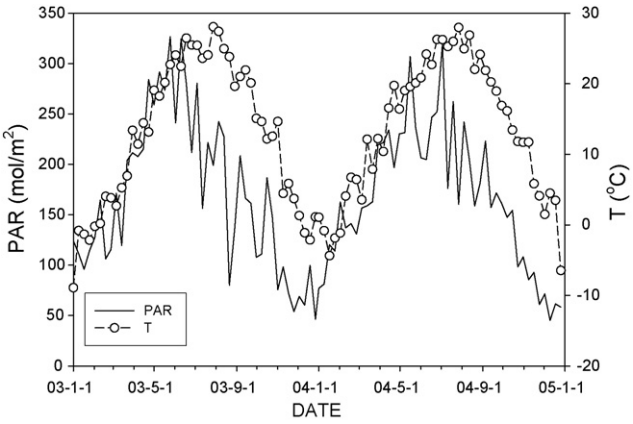

Fig. 1. Seasonal dynamics of air temperature and photosynthetically active radiation (PAR) in 2003 and 2004 at Yucheng, Shangdong Province, China.

2.2. Site-specific climate data and CO_2 flux measurement

A variety of meteorological measurements, including daily maximum temperature, daily minimum temperature, soil temperature (°C) and daily sum of photosynthetically active radiation (PAR, mol/(m^2 day)), are available for this study. Daily PAR and mean temperature data were used for simulation of the VPM model with daily MODIS data. In order to run the VPM model with 8-day MODIS data, both daily climate data (PAR and mean daytime temperature) and CO_2 flux data were aggregated to 8-day intervals (consistent with the days used in MODIS 8-day composite data). The mean of daily daytime mean temperature and the sums of PAR and CO_2 flux over 8-day periods were calculated (Fig. 1).

Evaluating GPP estimates at canopy level is a challenging task. Recent progress in partitioning of observed NEE data into GPP and ecosystem respiration (Re) make it possible to directly evaluate GPP estimates from various models. Daily flux data of NEE, GPP and ecosystem respiration (Re) at the individual flux sites were generated from the half-hourly flux data. Half-hourly values were calculated from the covariance of the fluctuations in vertical wind speed and CO_2 concentration measured at 5 Hz. We calculated the 8-day sums of GPP and NEE from the daily GPP and NEE data, in order to be consistent with the 8-day composite satellite images.

2.3. Estimation of GPP flux from eddy flux tower data

Canopy CO_2 and H_2O fluxes over winter wheat and maize were continuously measured by the eddy covariance (EC) system at Yucheng station during 2003–2004 as part of the Chinese Terrestrial Ecosystem Flux Observation and Research Network (ChinaFLUX) (Li et al., 2006; Yu et al., 2006). The EC system consists of a three-dimensional sonic anemometer (model CSAT3, Campbell Sci., Logan, UT) and an open-path infrared CO_2/H_2O analyzer (IRGA, Li-7500, Li-Cor Inc., Lincoln, Nebraska, USA) at a height of 2.80 m, which measures fluctuations of wind velocity, temperature, water vapor and CO_2 concentrations at 10 Hz, with CO_2 and H_2O fluxes averaged at 0.5 h intervals.

The measured net ecosystem CO_2 exchange (NEE) was calculated with corrections for tilt effect, canopy storage and density effects due to heat and water vapor transfer (Webb et al., 1980; Wilczak et al., 2001). We rejected anomalous or spurious values of NEE due to sensor malfunction, rain events, and interference from dew, hoarfrost and birds, etc. The measured NEE under stable conditions during nighttime (with friction velocity u^*<0.15 m s^{-1}) were also rejected. More details on data treatments have been described in other papers (Li et al., 2006; Yu et al., 2006; Zhao et al., 2007).

To create complete data sets for calculation of daily and annual sums of NEE and GPP, the data gaps were filled using several strategies suggested by Falge et al. (2001) and Reichstein et al. (2005). For small gaps (<2 h), the missing data was linearly interpolated. For larger gaps, the daytime data gaps were estimated as a function of PAR with the Michaelis–Menten equation (Falge et al., 2001), and the nighttime data gaps were filled by using the empirical relationships between ecosystem respiration and soil temperature under high turbulence (Lloyd and Taylor, 1994). Daytime respiration ($R_{eco,day}$) was estimated by extrapolating the relationship between nighttime respiration and soil temperature to daytime(Hu et al., 2008).

Gross ecosystem production (GPP) was derived by subtracting the daytime respiration ($R_{eco,day}$) from the corresponding daytime NEE:

$$GPP = NEE - R_{eco,day} \quad (1)$$

Daily GPP data were aggregated to 8-day intervals to be consistent with MODIS 8-day composites.

3. Description of the VPM model

3.1. Model structure

Vegetation canopies are composed of photosynthetically active vegetative parts (mostly chlorophyll) and non-photosynthetically active vegetative parts (NPV, mostly senescent foliage, branches and stems). NPV has a significant effect on FPAR at the canopy level (Asner et al., 1998). Light absorption of nonphotosynthetic components within a leaf varies in magnitude depending on species, leaf morphology, leaf age, and growth history (Hanan et al., 1998; Lambers et al., 1998; Hanan et al., 2002). For row crops, during the reproductive stage and at the beginning of senescence stage the fraction of photosynthetically active radiation absorbed by the vegetation canopy ($FPAR_{canopy}$) remains almost insensitive to reduction in chlorophyll (Chl), especially in maize (Vina et al., 2004). A likely explanation is that during the reproductive and senescence stages, the canopy still intercepts incoming radiation, but the leaves contain less photosynthetic pigments (Hatfield et al., 1984; Gallo et al., 1985). Since only the chlorophyll component of the canopy is used for photosynthesis, $FPAR_{canopy}$ needs to be partitioned into the fraction of PAR absorbed by chlorophyll ($FPAR_{chl}$) and the fraction of PAR absorbed by non-photosynthetically active components ($FPAR_{npv}$). The VPM was built upon the conceptual partitioning of chlorophyll ($FPAR_{chl}$) and non-photosynthetically active vegetation (NPV) within the canopy, and it estimates GPP over the photosynthetically active period of vegetation (Xiao et al., 2004a). The function used in the VPM for estimation of GPP is

$$GPP = \varepsilon_g \times FPAR_{chl} \times PAR \quad (2)$$

where $FPAR_{chl}$ is the fraction of photosynthetically active radiation (PAR) absorbed by leaf chlorophyll in the canopy, PAR is the photosynthetically active radiation (μmol photosynthetic photon flux density, PPFD), and ε_g is the light use efficiency (μmol CO_2/μmol PPFD).

In this version of the VPM model, $FPAR_{chl}$ within the photosynthetically active period of vegetation is estimated as a linear function of enhanced vegetation index (EVI), and the coefficient a is set to be 1.0 (Xiao et al., 2004a,b):

$$FPAR_{chl} = a \times EVI \quad (3)$$

Light use efficiency (ε_g) is affected by temperature, water, and leaf phenology:

$$\varepsilon_g = \varepsilon_0 \times T_{scalar} \times W_{scalar} \times P_{scalar} \quad (4)$$

where ε_0 is the apparent quantum yield or maximum light use efficiency (μmol CO_2/μmol PPFD), and T_{scalar}, W_{scalar} and P_{scalar} are the scalars for the effects of temperature, water and leaf phenology on light use efficiency of vegetation, respectively (Xiao et al., 2004a,b, 2005a,b).

3.2. Vegetation indices used as model input data

The satellite-based VPM model uses two vegetation indices as input data: EVI and land surface water index (LSWI). EVI directly adjusts the reflectance in the red band as a function of the reflectance in the blue band (ρ_{blue}), accounting for residual atmospheric contamination (e.g., aerosols), variable soil and canopy background reflectance (Huete et al., 1997):

$$EVI = \frac{G \times (\rho_{nir} - \rho_{red})}{(\rho_{nir} + (C_1 \times \rho_{red} - C_2 \times \rho_{blue}) + L)} \quad (5)$$

where G = 2.5, C_1 = 6, C_2 = 7.5, and L = 1; ρ_{nir}, ρ_{red} and ρ_{blue} is the reflectance of the blue, red and near infrared bands.

As the short infrared (SWIR) spectral band is sensitive to vegetation water content and soil moisture, a combination of NIR and SWIR bands has been used to derive water-sensitive vegetation indices (Gao, 1996; Ceccato et al., 2001, 2002a,b). LSWI is calculated as the normalized difference between NIR and SWIR spectral bands (Xiao et al., 2002):

$$LSWI = \frac{(\rho_{nir} - \rho_{swir})}{(\rho_{nir} + \rho_{swir})} \quad (6)$$

where $\rho_{nir}$and ρ_{swir} is reflectance of the near infrared bands and short infrared bands.

EVI and LSWI have been widely used to characterize the growing conditions of vegetation (Zhang et al., 2003; Boles et al., 2004). The EVI and LSWI are two vegetation indices that differ from widely used normalized difference vegetation index (NDVI). NDVI was often applied in production efficiency models to estimate vegetation productivity of terrestrial ecosystems (Field et al., 1995; Prince and Goward, 1995; Nemani et al., 2003):

$$NDVI = \frac{(\rho_{nir} - \rho_{red})}{(\rho_{nir} + \rho_{red})} \quad (7)$$

However, it is known that NDVI suffers several limitations, including sensitivity to atmospheric conditions, soil background (e.g., soil moisture), and saturation of NDVI values in multi-layered and closed canopies (Huete et al., 2002; Xiao et al., 2004a,b).

Satellite images from the MODIS onboard Terra satellite have blue, red, near infrared and shortwave infrared bands, which enable calculation of EVI and LSWI indices. The MODIS sensor acquires daily images at a spatial resolution of 250 m for red (620–670 nm) and near infrared (841–875 nm) bands, and at a spatial resolution of 500 m for blue (459–479 nm), green (545–565 nm), near infrared (1230–1250 nm) and shortwave infrared bands (1628–1652 nm, 2105–2155 nm). The MODIS Land Science Team

provides 8-day composite products for users (http://www.MODIS-land.gsfc.nasa.gov/), including the 8-day Land Surface Reflectance product (MOD09A1) that has the above-mentioned spectral bands. The MODIS sand surface reflectance data sets (MOD09A1) have a spatial resolution of 500 m. We obtained 8-day Land Surface Reflectance (MOD09-A1) data sets for 2003 and 2004 from the EROS Data Center, US Geological Survey (http://www.edc.usgs.-gov/). Reflectance values of the 8-day land surface reflectance data set from these four spectral bands (blue, red, near infrared (841–875 nm), and shortwave infrared (1628–1652 nm)) were used to calculate vegetation indices (NDVI, EVI and LSWI). For a time-series data of vegetation index, we used a simple method (Xiao et al., 2003) to fill vegetation index values for those cloudy pixels identified by the quality flag in the MOD09A1 files. We first selected a three-point time-series filter, $X(t-1)$, $X(t)$ and $X(t+1)$ and used values of noncloudy pixels in this window to correct a cloudy pixel. If both $X(t-1)$ and $X(t+1)$ pixels were cloudfree, we calculated the mean of $X(t-1)$ and $X(t+1)$, and used the mean value to replace $X(t)$. If only one pixel (either $X(t-1)$ or $X(t+1)$) was cloudfree, we used that pixel to replace $X(t)$. If the algorithm did not succeed in a three-point time-series filter, we then extended to a fivepoint time-series filter, $X(t-2)$, $X(t-1)$, $X(t)$, $X(t+1)$ and $X(t+2)$, using the same procedure as the above three-point time-series filter. Based on the geo-location information (latitude and longitude) of the CO_2 flux tower site, data of vegetation indices were extracted from one MODIS pixel that is centered on the flux tower.

4. Estimation of VPM model parameters

4.1. Estimating canopy-level maximum light use efficiency (ε_0) parameter

In the VPM model, the ecosystem-level ε_0 values vary with vegetation type. Information about ε_0 for individual vegetation types can be obtained from analysis of net ecosystem exchange (NEE) of CO_2 and incident PAR (μmol/(m^2 s)) at CO_2 eddy flux tower sites (Goulden et al., 1997). In order to estimate the ε_0 values of individual vegetation types, the Michaelis–Menten function (Eq. (8)) was used, based on the 10-day flux data at 30-min intervals over the peak period of the crop growing season in 2004:

$$\mathrm{NEE} = \left(\frac{\alpha \cdot PAR \times \mathrm{GPP_{max}}}{\alpha \cdot PAR + \mathrm{GPP_{max}}}\right) + R_{\mathrm{eco,day}} \quad (8)$$

where α is maximum light use efficiency or ecosystem apparent quantum yield (mg CO_2/μmol photon), and $\mathrm{GPP_{max}}$ is the ecosystem gross primary productivity at "saturating" light (mg CO_2/(m^2 s)). $R_{\mathrm{eco,day}}$ is daytime ecosystem respiration, and NEE is net ecosystem CO_2 exchange (both in mg CO_2/(m^2 s)) as measured by EC system.

From the calculated α time series with 10-day intervals in Yucheng, the maximum α value for winter wheat occurred in the end of April (0.76 gC/mol PAR) and the maximum α value for maize occurred in the beginning of September in 2004 (0.92 gC/mol PAR). The estimated maximum α values were used as estimates of the ε_0 parameter for winter wheat and maize in the VPM model.

4.2. Effect of temperature on GPP (T_{scalar})

Temperature affects photosynthesis, and there are a number of ways to estimate the effect of temperature on photosynthesis (T_{scalar}). In the VPM model, T_{scalar} is estimated at each time step, using the equation developed for the terrestrial ecosystem model (Raich et al., 1991):

$$T_{scalar} = \frac{(T - T_{min})(T - T_{max})}{[(T - T_{min})(T - T_{max})] - (T - T_{opt})^2} \quad (9)$$

where T_{min}, T_{max} and T_{opt} are the minimum, maximum and optimal temperature for photosynthetic activities, respectively. If air temperature falls below T_{min}, T_{scalar} is set to be zero. T_{min}, T_{max} and T_{opt} parameters vary depending on crop type. T_{min} and T_{max} values are set to −3 and 42 °C for winter wheat (Arora, 2003), and 0 and 45 °C for maize (Hirasawa and Hsiao, 1999). The optimum temperature (T_{opt}) is defined as the long-term mean temperature for the growing season, based on the concept that plants grow efficiently at the prevailing temperature (Sellers et al., 1992; Cao et al., 2004).

4.3. Effect of water on GPP (W_{scalar})

For W_{scalar}, the effect of water on plant photosynthesis, the availability of time-series data of SWIR and NIR bands from the new generation of advanced optical sensors (e.g. VGT, MODIS) offers opportunities for quantifying canopy water content at large spatial scales through the vegetation indices approach (Ceccato et al., 2002b). Vegetation indices that are based on NIR and SWIR bands are sensitive to change in equivalent water thickness (g/cm^2) at leaf and canopy levels (Hunt and Rock, 1989; Ceccato et al., 2001, 2002a,b). The VPM model uses a satellite-derived LSWI to estimate the seasonal dynamics of W_{scalar}:

$$W_{scalar} = \frac{1 + LSWI}{1 + LSWI_{max}} \quad (10)$$

where $LSWI_{max}$ is the maximum LSWI during the growing season for individual pixels. Estimation of site-specific $LSWI_{max}$ is dependent upon the time series of remote sensing data. The maximum LSWI value for the growing season was selected as an estimate of $LSWI_{max}$ (Xiao et al., 2004a,b, 2005a,b). Based on the analysis of LSWI seasonal dynamics derived from MODIS image data from 2003 to 2004, we used 0.34 for $LSWI_{max}$ of the winter wheat season and 0.39 for $LSWI_{max}$ of the maize season.

4.4. Effect of leaf phenology (P_{scalar})

Leaf age affects the seasonal patterns of photosynthetic capacity and net ecosystem exchange of carbon in a deciduous forest (Wilson et al., 2001). In the VPM model, P_{scalar} is included to account for the effect of leaf age on photosynthesis at canopy level, and calculation of P_{scalar} is dependent upon leaf longevity.

For maize, an obvious leaf expansion phase can be identified over the plant growing season, so maize phenology is generally divided into vegetative (from emergence to tasseling according to the number of fully expanded leaves) and reproductive (from silking to physiological maturity according to the degree of kernel development) stages (Ritchie et al., 1992; Vina et al., 2004). For maize, P_{scalar} is calculated at two different phases:

$$P_{scalar} = \frac{1 + LSWI}{2} \quad \text{during emergence to leaf full expansion} \quad (11)$$

$$P_{scalar} = 1 \quad \text{after leaf full expansion.} \quad (12)$$

Winter wheat has new leaves emerging throughout much of the plant growing season. Moreover, the intercepted PAR was derived from the 2 to 3 most tender leaves in the top of the canopy during later stages (Monteith, 1994), so the P_{scalar} is set to 1.0 (Xiao et al., 2005a; Li et al., 2006, 2007).

Earlier studies have indicated that time series of greenness-related vegetation indices (e.g., NDVI, EVI) and water-related vegetation indices (LSWI) can be used to identify the green-up phase (from the beginning of leaf budding to the completion of full leaf expansion) and senescence/leaf-drop phase at the canopy level (Xiao et al., 2002). LSWI values range from −1 to +1 (a range of 2), and the simplest formulation of P_{scalar} (Eq. (11)) is a linear scalar with a value range of 0–1. The green-up period for the calculation of P_{scalar} is defined as the period from the date that had the minimum LSWI to the date that had the maximum LSWI in each crop growth season.

5. Results

5.1. Seasonal dynamics of NDVI, EVI and LSWI for winter wheat–maize double-cropping land

The time series of MODIS composite images at 8-day intervals provides dynamic vegetation information and can be used to identify key phenology transition dates or perform vegetation phenology mapping (Zhang et al., 2003, 2006; Sakamoto et al., 2005), crop intensity (number of crop cultivation seasons in 1 year) and crop calendar therefore can be detected from the crop growth curves. NDVI and EVI time series from 2002 to 2004 both exhibit bimodal temporal curves corresponding to the winter wheat–maize double-cropping system. NDVI and EVI values started to increase as winter wheat recovered with increasing temperatures and reached a plateau value in mid-April, then decreased and fell sharply as the crop reached maturity. A similar EVI and NDVI crop growth curve was exhibited from June to September as summer maize progressed from budding to maturity (Fig. 2). NDVI and EVI dynamics during the winter wheat season at the double-cropping site differ substantially from maize in terms of phase and magnitude (Fig. 2a and b). The maximum EVI values in winter wheat season were 0.41, 0.47 and 0.46 from the years 2002 to 2004, while the maximum NDVI values were 0.56, 0.56 and 0.61, about 20% lower than the maximum EVI (0.66, 0.76 and 0.67) and NDVI values (0.77, 0.86, and 0.90) during the maize season in the three observational years, respectively. The time series of LSWI data also have two distinct seasonal cycles for winter wheat and maize growth (Fig. 2c). The maximum LSWI values in the winter wheat season were 0.23, 0.28 and 0.34 from 2002 to 2004, while in the maize season the maximum values were 0.31, 0.38 and 0.39.

EVI and NDVI curves both changed significantly over time and exhibited quite different temporal patterns during the winter wheat and summer maize seasons. The comparison between the vegetation index curves and observed crop phenology data at the Yucheng site in 2002 provided an explicit interpretation (Fig. 3). In winter wheat season, NDVI and EVI values begin to gradually increase as winter wheat recovers along with increased temperatures. EVI was reaching a plateau value after wheat jointing and then reached its peak at the heading stage in mid-April; it took about 70 days from recovering to heading and 20 days from jointing to heading. NDVI maintained a longer plateau value stage than EVI because NDVI values were saturated in well-vegetated areas, for a period of about 30 days. NDVI was reaching the plateau value at wheat jointing time, and lasted until 10 days after heading. After heading, EVI decreased sharply to the minimum and reached maturity 45 days later. NDVI also sharply decreased from peak value to minimum value within around 40 days.

In the maize season, EVI and NDVI reached a plateau value more rapidly than winter wheat. It took 50 days from emergence to heading. EVI reached the peak value at the time of maize jointing and then gradually decreased. NDVI reached a higher value after jointing and maintained a longer plateau until 10 days prior to maturity. The period of NDVI saturation in the summer maize season was almost 60 days, which covered nearly 60% of the full season and was over 20 days longer than the NDVI saturation period of winter wheat because the canopy of maize is much denser than wheat.

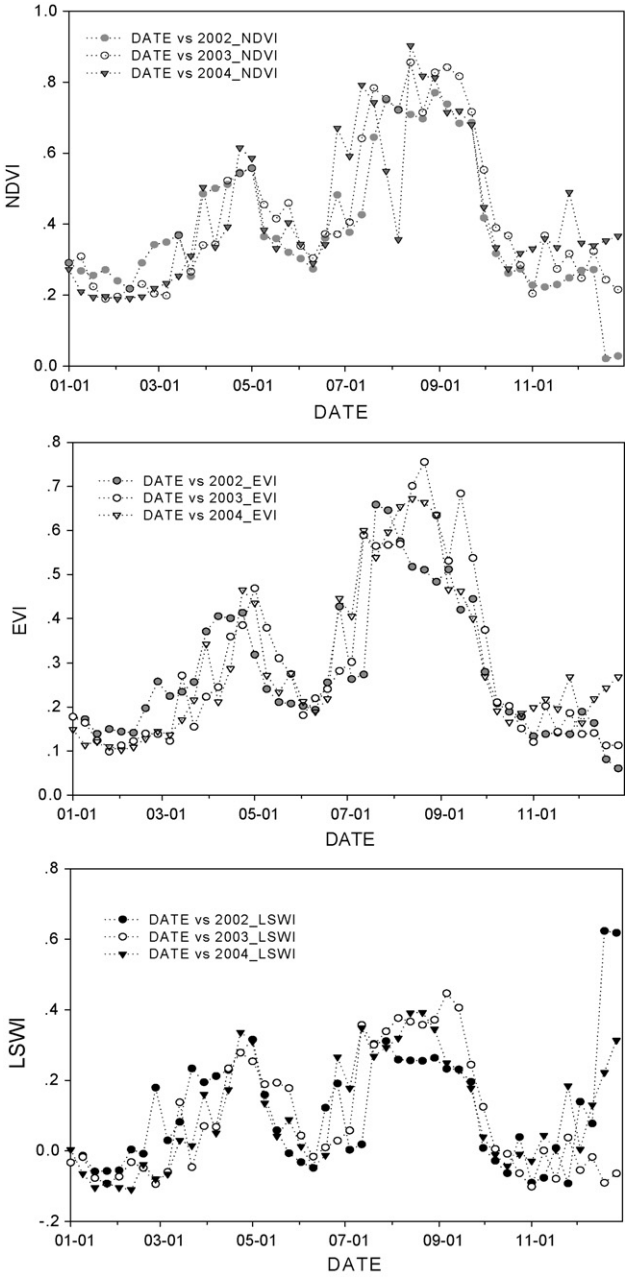

Fig. 2. Seasonal dynamics of NDVI, EVI, LSWI from 2002–2004.

LSWI also exhibited a seasonal cycle with crop planting and harvest, but it did not change over time as significantly as NDVI and EVI during the period from canopy development to leaf senescence (especially in the maize growth season), and overall maintained a higher value which fluctuated some with water stress. As the crop was reaching maturity, LSWI sharply decreased and then fell to minimum values (close to zero) once the crop was mature. The difference between EVI and NDVI was remarkable during the period of flourishing crop growth. One important reason for this was that the NDVI values were saturated when the vegetation canopy was fully developed as the LAI was relatively high. EVI does

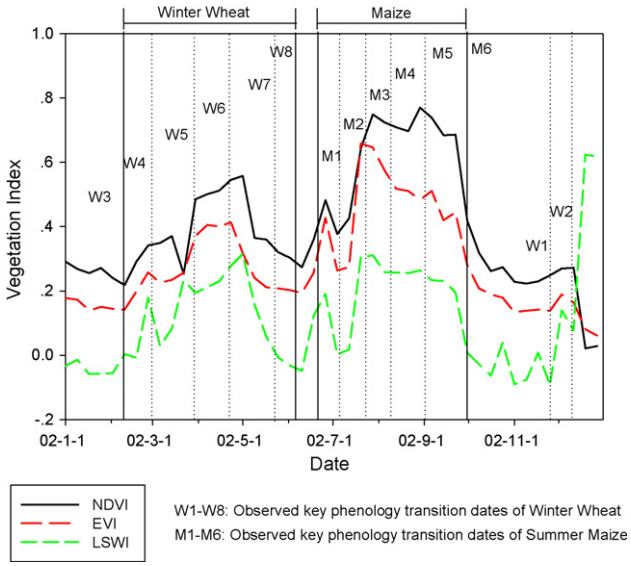

Fig. 3. Winter wheat–maize phenology and vegetation index in Yucheng. W1: winter wheat emergence; W2: winter wheat dormancy; W3: winter wheat recovery; W4: winter wheat tillering; W5: winter wheat jointing; W6: winter wheat heading; W7: winter wheat milking; W8: winter wheat maturity. M1: maize emergence; M2: maize–seven leaves; M3: maize jointing; M4: maize heading; M5: maize milking; M6: maize maturity.

not appear to be as saturated as NDVI. Thus, EVI provides more accurate crop growing information on canopy and leaf activity than does NDVI during stages of flourishing growth. Nevertheless, the remarkable differences between them also suggest that we could use them to identify leaf phenology, because the occurrence of NDVI saturation was closely linked to the jointing stage. LSWI is sensitive to initiation of crop leaf senescence, so the seasonal dynamic of LSWI is more relevant for identifying the crop maturity date than EVI and NDVI.

The observed key transition dates of crop growth stages during 2003 and 2004 indicated (Tables 1 and 2) that there was little variation in both winter wheat and maize for the four observed transition dates from 2002 to 2004, except the recovery and jointing dates of winter wheat in 2004 were earlier than in 2002 and 2003 because winter wheat recovery is sensitive to temperature trends, which also could be detected from EVI and NDVI curves (Fig. 2).

5.2. GPP dynamics and crop phenology

Fig. 4 shows that the NEE and GPP time series in 2003 and 2004 for the Yucheng double-cropping ecosystem had two distinct crop

Table 1
The phenological transition dates of winter wheat in Yucheng during 2002–2004.

Year	Revival date	Jointing date	Heading date	Maturity date
2002	7 February 2002	28 March 2002	18 April 2002	3 June 2002
2003	13 February 2003	25 March 2003	28 April 2003	4 June 2003
2004	1 February 2004	9 March 2004	23 April 2004	4 June 2004

Table 2
The phenological transition dates of maize in Yucheng during 2002–2004.

Year	Emergence date	Jointing date	Heading date	Maturity date
2002	18 June 2002	24 July 2002	8 August 2002	30 September 2002
2003	24 June 2003	25 July 2003	13 August 2003	30 September 2003
2004	26 June 2004	21 July 2004	9 August 2004	2 October 2004

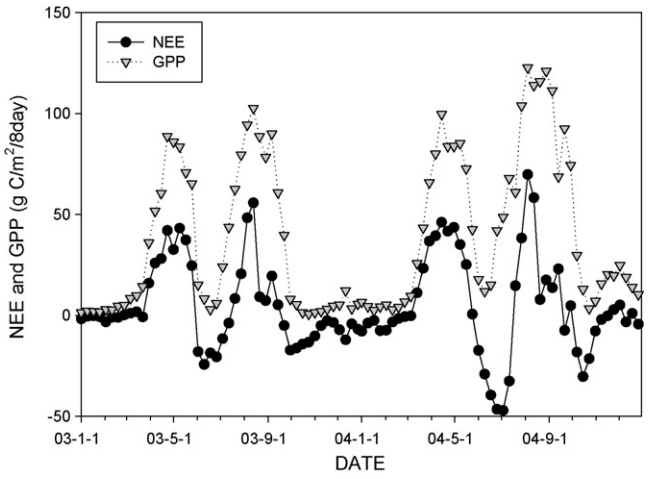

Fig. 4. Seasonal dynamics of GPP and NEE during 2003 and 2004.

growth cycles. In contrast to most natural ecosystems, the seasonal dynamics of GPP cannot be explained by the seasonal dynamics of air temperature and PAR (Li et al., 2007), because the vegetation growth within the intensified cropland is highly influenced by humans. The maximum GPP values were ~89 gC/m^2/8-day in the winter wheat season and ~103 gC/m^2/8-day in the maize season. There were two obvious stages when GPP values were near zero. One is in the winter season, after the maize harvest at the end of September. GPP showed little increase during winter wheat emergence and growth after late November, subsequently low air temperatures inhibited photosynthetic activities and caused dormancy in the winter wheat from early December until temperatures increased in February. The second stage is the transition phase (2 weeks) between winter wheat and maize seasons in mid-June, because the cropland surface has no vegetation cover between the winter wheat harvest and maize emergence. For the first crop cycle, GPP began to increase in late February (winter wheat recovery) and rose rapidly from late March (wheat jointing) to mid-April (wheat heading), which corresponds to the vegetative stages. During this phase most photosynthetic production was directed to leaf development. GPP declined rapidly after its peak in mid-April and then fell to zero (wheat maturity) by the end of May. The second cycle started in early June (maize emergence) and rapidly climbed to a peak in early August, falling to zero when maize matured at the end of September. Maize has a higher photosynthetic capability, as its peak value of GPP during the maize season was 102.6 gC/m^2/8-day and 122.7 gC/m^2/8-day in 2003 and 2004, respectively, while the peak value was only 88.7 gC/m^2/8-day and 99.6 gC/m^2/8-day in the winter wheat season.

5.3. Seasonal dynamics of predicted CO_2 fluxes from the VPM model

The VPM model was run using site-specific data on temperature, PAR and vegetation indices in 2003–2004. The seasonal dynamics of predicted GPP (GPP_{pred}) from the VPM model were compared with the observed GPP (GPP_{obs}) data for 8-day intervals over the period of winter wheat and maize seasons (Fig. 5). The seasonal dynamics of GPP_{pred} for both the winter wheat and maize seasons agreed reasonably well with those of GPP_{obs}. The simple linear regression model also shows a good agreement between GPP_{pred} and GPP_{obs} during the plant-growing season in 2003–2004 (Fig. 6). The comparison of annually integrated GPP from VPM and FLUX estimations is listed in Table 3. Annual GPP from FLUX estimation was 1409 and 2131 gC/m^2 in 2003 and 2004,

Table 3
Time integrated sums of gross primary production (GPP, gC/m^2).

Year	Tower data			VPM model		
	GPP_{obs} (1–12)	GPP_{obs} (winter wheat)	GPP_{obs} (maize)	GPP_{pred} (1–12)	GPP_{pred} (winter wheat)	GPP_{pred} (maize)
2003	1409.37	602.21	789.17	1624.76	637.04	928.26
2004	2131.83	728.80	1170.61	1745.97	560.56	1041.11

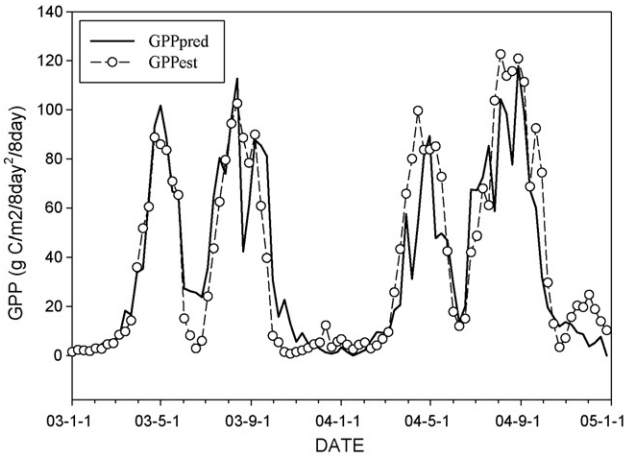

Fig. 5. Comparison of the seasonal dynamics of observed gross primary production (GPP) and predicted GPP during 2003–2004 at the eddy flux tower site at Yucheng winter wheat–maize double cropping system, Shandong Province, China. Solid line-GPPpred and open circle-GPPobs.

respectively, while annual GPP from VPM was 1624 and 1745 gC/m^2. The total GPP_{obs} of winter wheat season were 602 gC/m^2 in 2003 and 728 gC/m^2 in 2004, while the total GPP_{pred} were 637 gC/m^2 in 2003 and 560 gC/m^2 in 2004. The total GPP_{obs} of maize season were 789 gC/m^2 in 2003 and 1170 gC/m^2 in 2004, while the total GPP_{pred} were 928 gC/m^2 in 2003 and 1041 gC/m^2 in 2004. Total GPP_{pred} (gC/m^2) for both the winter wheat and maize seasons were higher than GPP_{obs} in 2003 and lower in 2004, with a minimum difference of 5.7% for the 2003 winter wheat season and a maximum difference of −23% in the 2004 winter wheat season. The GPP differences for the maize season between the VPM model and flux estimation were +17.6% and −11% in 2003 and 2004, respectively.

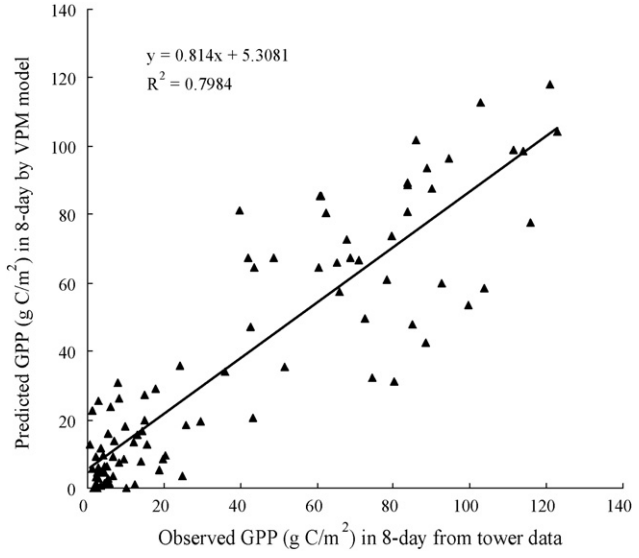

Fig. 6. Comparison between the observed gross primary production (GPP) and predicted GPP during 2003–2004 at the eddy flux tower site of Yucheng winter wheat–maize double cropping land, Shandong Province, China.

6. Discussion and conclusion

Seasonal C3 and C4 crop rotation in a single year (particularly winter wheat and maize double-cropping) is the most extensive type of intensified land use in the Huang-Huai-Hai plain (Xin et al., 2002). The results from flux tower measurement indicate that C4 plants have a higher maximum light use efficiency than C3 plants at the canopy level. Some studies had proved the significant dependence of LUE on photosynthesis pathways (Lobell et al., 2002). It has been recognized that monitoring phenology over wide areas is essential for crop yield modeling and estimation of net primary production (White et al., 1997; Sakamoto et al., 2005). However, multiple-cropping has not yet been considered as a land cover type in most land cover classification products or the input datasets of GPP models. The significant underestimation of GPP and disadvantage for global biogeochemical cycle and food security studies due to the omission of multiple cropping system has been highlighted in recent research (Zhang et al., 2008). In this study, we evaluated the phenological and biophysical performance of vegetation indices (NDVI, EVI and LSWI) and their relations to the GPP dynamics of a winter wheat–maize double-cropping system at Yucheng, China. The temporal consistency between the vegetation indices dynamics and phenological observation demonstrated that the combination of the three vegetation indices has the potential for detecting information on crop phenology and crop calendar that is important for estimation of GPP in human-managed ecosystems. The differences in magnitude and phase between the EVI and NDVI time series of winter wheat and maize suggest that maize and winter wheat can be spatially and temporally identified. Therefore, we can evaluate the model parameters for winter wheat and maize cropping seasons separately to estimate light use efficiency and temperature, water and leaf age convergent factors in the VPM model. The estimated maximum LUE α values from the flux tower during winter wheat and maize seasons were well within the range of reported α values for C3 and C4 crop canopies (α = 0.16–0.98 gC mol^{-1} PAR) (Singsaas et al., 2001). In the standard MODIS-based GPP/NPP algorithm (MOD17) (Running et al., 1999, 2000), which does not distinguish between C3 and C4 crops, the ε_0 value of crop is 0.68 gC/MJ (approximately 0.31–0.33 gC/mol PPFD), which was lower than the 0.76 gC/mol PPFD for winter wheat and 0.92 gC/mol PPFD for maize obtained here from the flux tower data, based on an approximate conversion of 2.05–2.17 between MJ (10^6 J) and mol PPFD (Weiss and Norman, 1985; Aber et al., 1996). Land use change, disturbance history, and different successional stages of vegetation may result in the spatial variation and temporal changes of ε_0 within a biome type. The estimation of the ε_0 parameter from analysis of gross ecosystem exchange of CO_2 and photosynthetic photon flux density (PPFD) at a CO_2 eddy flux tower site is also largely determined by the choice of either a linear or nonlinear model (e.g., hyperbolic equation) between GPP and

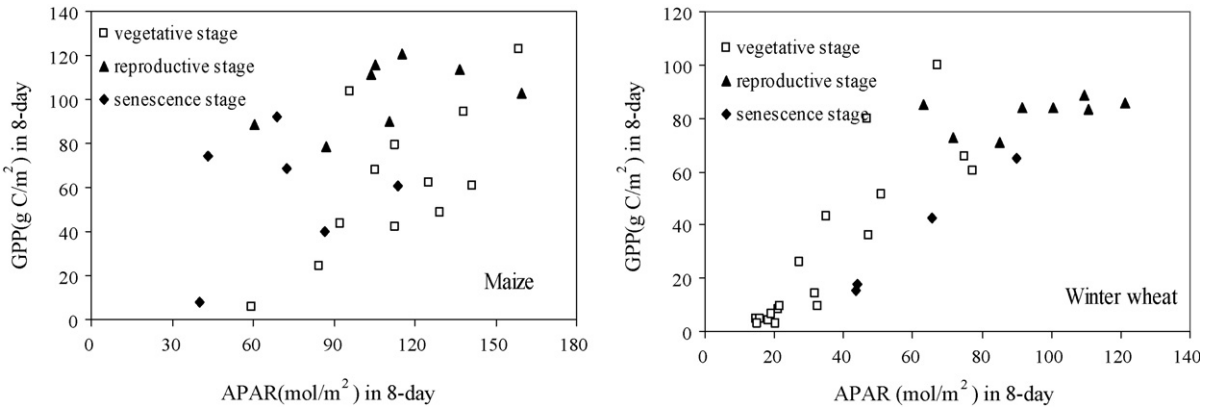

Fig. 7. The relationship between GPP and absorbed photosynthetically active radiation (APAR) calculated as APAR = fAPAR × PAR for (A) winter wheat and (B) maize in 2003–2004.

absorbed PAR data over a growing season (Xiao, 2006), which would result in ε_0 value difference between different ε_0 methods even if the flux tower site was at same location.

Crop photosynthetic activity changes with canopy leaf age, because as the crop goes through phenological evolution (vegetative, reproductive and senescence stages), crop leaves change in their biophysical (e.g., LAI, fPAR) and biochemical (e.g., chlorophyll and other pigments, nitrogen) properties (Gitelson et al., 2005, 2006). Leaf development is quite different for maize and winter wheat because tillering and leaf growth last for nearly the entire winter wheat season, while maize exhibits a distinct leaf expansion phase (vegetative stage) (Smith and Hamel, 1999; Vina et al., 2004). The maize LAI therefore increases more rapidly during the vegetative growth stages and approaches to peak value a month earlier compared to the winter wheat canopy. To evaluate the algorithms of P_{scalar} in VPM for the crop GPP modeling, we analyzed the relationship between observed GPP and APAR (calculated as the product of FPAR and PAR) and plotted this versus GPP (Fig. 7). The behavior of GPP versus APAR was different for winter wheat and maize at vegetative, reproductive and senescence stages. For winter wheat, GPP was almost linearly related with APAR with the same slope and intercept across vegetative, reproductive and senescence stages. In contrast, no clear relationship was observed during the maize season. The relationship between GPP and APAR was close to linear at vegetative stage and senescence stages, while GPP almost did not change with APAR at reproductive stage, but with much lower light use efficiency during the vegetative stage than during the reproductive stage, which indicates that P_{scalar} should be calculated for two different phases.

The results of the VPM model simulations showed that in general, there is good agreement between GPP_{pred} and GPP_{obs} for the photosynthetically active period during 2003–2004 in the double cropping site. However, there still exist large differences between GPP_{obs} and GPP_{pred} during a few 8-day periods (Fig. 5), such as smaller GPP_{pred} in late August in 2003 and 2004, and in early April and late July in 2004. The large discrepancies between GPP_{obs} and GPP_{pred} may be attributed to three sources of errors. The first source is the sensitivity of the VPM model to PAR, for instance, smaller GPP_{pred} in DOY 209–217 and DOY 233–241 in 2004. The second source is the error (overestimation or underestimation) of observed GPP (GPP_{obs}). GPP_{obs} is calculated from flux-measured NEE and estimated daytime ecosystem respiration. The two major steps that must be taken to calculate GPP are the filling of data gaps for NEE and estimation of daytime (solar altitude >0) ecosystem respiration. Both of these steps require subjective decisions and are currently the subject of a great deal of discussion (Falge et al., 2002a,b). The third source is the time-series data of vegetation indices derived from satellite images. We used the 8-day MODIS composite images that have no BRDF correction or normalization, and thus the effect of angular geometry on surface reflectance and vegetation indices remained. We suggest that future field work should focus on measurements of leaf water content, chlorophyll and dry matter during every key crop phenological transition stage, to improve understanding of temporal processes of vegetation indices dynamics (e.g., EVI and LSWI) and in-depth studies on model improvement.

In summary, this study has explored the potential of 8-day composite MODIS vegetation indices for improving seasonal characterization of leaf phenology and canopy water content of multiple cropping. It has also demonstrated the potential of the VPM model for estimating GPP in a double-cropping system with C3 and C4 crop rotation. The results of this study are likely to have significant implications for remote sensing analyses of multiple-cropping agricultural systems, the carbon cycle and climate modeling.

Acknowledgments

This study was funded by the National Science Foundation of China (Grant No. 40601064), The Open-ended fund of State Key lab of Resources and Environmental Information System, National Key Project of Scientific and Technical Supporting Programs (No. 2006BAC08B03 and 2006BAC08B06), the International Partnership Project of CAS on "Human Activities and Ecosystem Changes" (Grant No. CXTD-Z2005-1), and NASA Land Cover and Land Use Change Program (NNH04ZYS005N and NNG05GH80G). We thank Drs. Jun Li and Fenghua Zhao for their field assistance.

References

Aber, J.D., Reich, P.B., Goulden, M.L., 1996. Extrapolating leaf CO_2 exchange to the canopy: a generalized model of forest photosynthesis compared with measurements by eddy correlation. Oecologia 106, 257–265.

Arora, V.K., 2003. Simulating energy and carbon fluxes over winter wheat using coupled land surface and terrestrial ecosystem models. Agric. For. Meteorol. 118, 21–47.

Asner, G.P., Bateson, C.A., Privette, J.L., El Saleous, N., Wessman, C.A., 1998. Estimating vegetation structural effects on carbon uptake using satellite data fusion and inverse modeling. J. Geophys. Res. [Atmos.] 103, 28839–28853.

Boles, S., Xiao, X., Liu, J., Zhang, Q., Munkhtuya, S., Chen, S., Ojima, D., 2004. Land cover characterization of temperate East Asia using multi-temporal VEGETATION sensor data. Remote Sens. Environ. 90, 477–489.

Bradford, J.B., Hicke, J.A., Lauenroth, W.K., 2005. The relative importance of light-use efficiency modifications from environmental conditions and cultivation for estimation of large-scale net primary productivity. Remote Sens. Environ. 96, 246–255.

Bricklemyer, R.S., Lawrence, R.L., Miller, P.R., Battogtokh, N., 2007. Monitoring and verifying agricultural practices related to soil carbon sequestration with satellite imagery. Agric. Ecosyst. Environ. 118, 201–210.
Cao, M.K., Prince, S.D., Small, J., Goetz, S.J., 2004. Remotely sensed interannual variations and trends in terestrial net primary productivity 1981–2000. Ecosystems 7, 233–242.
Ceccato, P., Flasse, S., Tarantola, S., Jacquemoud, S., Gregoire, J.M., 2001. Detecting vegetation leaf water content using reflectance in the optical domain. Remote Sens. Environ. 77, 22–33.
Ceccato, P., Flasse, S., Gregoire, J.M., 2002a. Designing a spectral index to estimate vegetation water content from remote sensing data—Part 2. Validation and applications. Remote Sens. Environ. 82, 198–207.
Ceccato, P., Gobron, N., Flasse, S., Pinty, B., Tarantola, S., 2002b. Designing a spectral index to estimate vegetation water content from remote sensing data: part 1—theoretical approach. Remote Sens. Environ. 82, 188–197.
Falge, E., Baldocchi, D., Olson, R., Anthoni, P., Aubinet, M., Bernhofer, C., Burba, G., Ceulemans, R., Clement, R., Dolman, H., Granier, A., Gross, P., Grunwald, T., Hollinger, D., Jensen, N.O., Katul, G., Keronen, P., Kowalski, A., Lai, C.T., Law, B.E., Meyers, T., Moncrieff, H., Moors, E., Munger, J.W., Pilegaard, K., Rannik, U., Rebmann, C., Suyker, A., Tenhunen, J., Tu, K., Verma, S., Vesala, T., Wilson, K., Wofsy, S., 2001. Gap filling strategies for defensible annual sums of net ecosystem exchange. Agric. For. Meteorol. 107, 43–69.
Falge, E., Baldocchi, D., Tenhunen, J., Aubinet, M., Bakwin, P., Berbigier, P., Bernhofer, C., Burba, G., Clement, R., Davis, K.J., Elbers, J.A., Goldstein, A.H., Grelle, A., Granier, A., Guomundsson, J., Hollinger, D., Kowalski, A.S., Katul, G., Law, B.E., Malhi, Y., Meyers, T., Monson, R.K., Munger, J.W., Oechel, W., Paw, K.T., Pilegaard, K., Rannik, U., Rebmann, C., Suyker, A., Valentini, R., Wilson, K., Wofsy, S., 2002a. Seasonality of ecosystem respiration and gross primary production as derived from FLUXNET measurements. Agric. For. Meteorol. 113, 53–74.
Falge, E., Tenhunen, J., Baldocchi, D., Aubinet, M., Bakwin, P., Berbigier, P., Bernhofer, C., Bonnefond, J.M., Burba, G., Clement, R., Davis, K.J., Elbers, J.A., Falk, M., Goldstein, A.H., Grelle, A., Granier, A., Grunwald, T., Gudmundsson, J., Hollinger, D., Janssens, I.A., Keronen, P., Kowalski, A.S., Katul, G., Law, B.E., Malhi, Y., Meyers, T., Monson, R.K., Moors, E., Munger, J.W., Oechel, W., Paw, U.K.T., Pilegaard, K., Rannik, U., Rebmann, C., Suyker, A., Thorgeirsson, H., Tirone, G., Turnipseed, A., Wilson, K., Wofsy, S., 2002b. Phase and amplitude of ecosystem carbon release and uptake potentials as derived from FLUXNET measurements. Agric. For. Meteorol. 113, 75–95.
Field, C.B., Randerson, J.T., Malmstrom, C.M., 1995. Global net primary production—combining ecology and remote-sensing. Remote Sens. Environ. 51, 74–88.
Gallo, K., Daughtry, C., Bauer, M., 1985. Spectral estimation of absorbed photosynthesis active radiation in corn canopies. Remote Sens. Environ. 17, 221–232.
Gao, B.C., 1996. NDWI—a normalized difference water index for remote sensing of vegetation liquid water from space. Remote Sens. Environ. 58, 257–266.
Gitelson, A.A., Vina, A., Ciganda, V., Rundquist, D.C., Arkebauer, T.J., 2005. Remote estimation of canopy chlorophyll content in crops. Geophys. Res. Lett. 32, L08403, doi:10.1029/2005GL022688.
Gitelson, A.A., Vina, A., Verma, S.B., Rundquist, D.C., Arkebauer, T.J., Keydan, G., Leavitt, B., Ciganda, V., Burba, G.G., Suyker, A.E., 2006. Relationship between gross primary production and chlorophyll content in crops: implications for the synoptic monitoring of vegetation productivity. J. Geophys. Res. [Atmos.] 111, D08S11, doi:10.1029/2005JD006017.
Goulden, M.L., Daube, B.C., Fan, S.M., Sutton, D.J., Bazzaz, A., Munger, J.W., Wofsy, S.C., 1997. Physiological responses of a black spruce forest to weather. J. Geophys. Res. [Atmos.] 102, 28987–28996.
Gower, S.T., Kucharik, C.J., Norman, J.M., 1999. Direct and indirect estimation of leaf area index, fAPAR, and net primary production of terrestrial ecosystems. Remote Sens. Environ. 70, 29–51.
Hanan, N., Kabat, P., Dolman, A.J., Elbers, J.A., 1998. Photosynthesis and carbon balance of a Sahelian fallow savanna. Global Change Biol. 4, 523–538.
Hanan, N.P., Burba, G., Verma, S.B., Berry, J.A., Suyker, A., Walter-Shea, E.A., 2002. Inversion of net ecosystem CO_2 flux measurements for estimation of canopy PAR absorption. Global Change Biol. 8, 563–574.
Hatfield, J.L., Asrar, G., Kanemasu, E.T., 1984. Intercepted photosynthetically active radiation estimated by spectral reflectance. Remote Sens. Environ. 14, 65–75.
Hirasawa, T., Hsiao, T.C., 1999. Some characteristics of reduced leaf photosynthesis at midday in maize growing in the field. Field Crops Res. 62, 53–62.
Hu, Z., Yu, G., Fu, Y., Sun, X., Li, Y., Shi, P., Wang, Y., Zheng, Z., 2008. Effects of vegetation control on ecosystem water use efficiency within and among four grassland ecosystems in China. Global Change Biol. 14, 1609–1619.
Huete, A.R., Liu, H.Q., Batchily, K., vanLeeuwen, W., 1997. A comparison of vegetation indices over a global set of TM images for EOS-MODIS. Remote Sens. Environ. 59, 440–451.
Huete, A., Didan, K., Miura, T., Rodriguez, E.P., Gao, X., Ferreira, L.G., 2002. Overview of the radiometric and biophysical performance of the MODIS vegetation indices. Remote Sens. Environ. 83, 195–213.
Hunt, E.R., Rock, B.N., 1989. Detection of changes in leaf water-content using near-infrared and middle-infrared reflectances. Remote Sens. Environ. 30, 43–54.
Lambers, H., Chapin, F.S., Pons, T.L., 1998. Plant Physiological Ecology. Springer-Verlag, New York.
Li, C.S., Zhuang, Y.H., Frolking, S., Galloway, J., Harriss, R., Moore, B., Schimel, D., Wang, X.K., 2003. Modeling soil organic carbon change in croplands of China. Ecol. Appl. 13, 327–336.
Li, J., Yu, Q., Sun, X.M., Tong, X.J., Ren, C.Y., Wang, J., Liu, E.M., Zhu, Z.L., Yu, G.R., 2006. Carbon dioxide exchange and the mechanism of environmental control in a farmland ecosystem in North China Plain. Sci. China Ser. D Earth Sci. 36, 226–240.
Li, Z., Yu, G., Xiao, X., Li, Y., Zhao, X., Ren, C., Zhang, L., Fu, Y., 2007. Modeling gross primary production of alpine ecosystems in the Qinghai-Tibet Plateau using MODIS images and climate data. Remote Sens. Environ. 107, 510–519.
Lloyd, J., Taylor, J.A., 1994. On the temperature-dependence of soil respiration. Function. Ecol. 8, 315–323.
Lobell, D.B., Hicke, J.A., Asner, G.P., Field, C.B., Tucker, C.J., Los, S.O., 2002. Satellite estimates of productivity and light use efficiency in United States agriculture, 1982–98. Global Change Biol. 8, 722–735.
Monteith, J., 1994. Validity of the correlation between intercepted radiation and biomass. Discussion. Agric. For. Meteorol. 68, 213–220.
Nemani, R.R., Keeling, C.D., Hashimoto, H., Jolly, W.M., Piper, S.C., Tucker, C.J., Myneni, R.B., Running, S.W., 2003. Climate-driven increases in global terrestrial net primary production from 1982 to 1999. Science 300, 1560–1563.
Prince, S.D., Goward, S.N., 1995. Global primary production: a remote sensing approach. J. Biogeogr. 22, 815–835.
Qiu, J., Tang, H., Frolking, S., Boles, S., Li, C., Xiao, X., Liu, J., Zhuang, Y., Qin, X., 2003. Mapping single-, double-, and triple-crop agriculture in China at 0.5°*0. 5° by combining county-scale census data with a remote sensing-derived land cover map. Geocarto Int. 18, 3–13.
Raich, J.W., Rastetter, E.B., Melillo, J.M., Kicklighter, D.W., Steudler, P.A., Peterson, B.J., Grace, A.L., Moore, B., Vorosmarty, C.J., 1991. Potential net primary productivity in South-America—application of a global-model. Ecol. Appl. 1, 399–429.
Reichstein, M., Falge, E., Baldocchi, D., Papale, D., Aubinet, M., Berbigier, P., Bernhofer, C., Buchmann, N., Gilmanov, T., Granier, A., Grunwald, T., Havrankova, K., Ilvesniemi, H., Janous, D., Knohl, A., Laurila, T., Lohila, A., Loustau, D., Matteucci, G., Meyers, T., Miglietta, F., Ourcival, J.M., Pumpanen, J., Rambal, S., Rotenberg, E., Sanz, M., Tenhunen, J., Seufert, G., Vaccari, F., Vesala, T., Yakir, D., Valentini, R., 2005. On the separation of net ecosystem exchange into assimilation and ecosystem respiration: review and improved algorithm. Global Change Biol. 11, 1424–1439.
Ritchie, S.W., Hanway, J.J., Benson, G.O., 1992. How a corn plant develops. Iowa State Univ. Sci. Tech. Cooperative Ext. Services. Report No. 48. Iowa State University, Ames.
Running, S.W., Nemani, R., Glassy, J.M., Thornton, P., 1999. MODIS Daily Photosynthesis (PSN) and Annual Net Primary Production (NPP) Product (MOD17), Algorithm Theorectical Basis Document. Version 3.0. April 29, 1999. http://modis.gsfc.nasa.gov/.
Running, S.W., Thornton, P.E., Nemani, R., Glassy, J.M., 2000. Global terrestrial gross and net primary productivity from the earth observing system. In: Sala, O.E., Jackson, R.B., Mooney, H.A., Howarth, R.W. (Eds.), Methods in Ecosystem Science. Springer-Verlag, New York, pp. 44–57.
Running, S.W., Nemani, R.R., Heinsch, F.A., Zhao, M.S., Reeves, M., Hashimoto, H., 2004. A continuous satellite-derived measure of global terrestrial primary production. Bioscience 54, 547–560.
Sakamoto, T., Yokozawa, M., Toritani, H., Shibayama, M., Ishitsuka, N., Ohno, H., 2005. A crop phenology detection method using time-series MODIS data. Remote Sens. Environ. 96, 366–374.
Sakamoto, T., Van Nguyen, N., Ohno, H., Ishitsuka, N., Yokozawa, M., 2006. Spatio-temporal distribution of rice phenology and cropping systems in the Mekong Delta with special reference to the seasonal water flow of the Mekong and Bassac rivers. Remote Sens. Environ. 100, 1–16.
Sellers, P.J., Berry, J.A., Collatz, G.J., Field, C.B., Hall, F.G., 1992. Canopy reflectance, photosynthesis, and transpiration. 3. A reanalysis using improved leaf models and a new canopy integration scheme. Remote Sens. Environ. 42, 187–216.
Singsaas, E.L., Ort, D.R., DeLucia, E.H., 2001. Variation in measured values of photosynthetic quantum yield in ecophysiological studies. Oecologia 128, 15–23.
Smith, D.L., Hamel, C., 1999. Crop Yield: Physiology and Processes. Springer-Verlag.
Soegaard, H., Jensen, N.O., Boegh, E., Hasager, C.B., Schelde, K., Thomsen, A., 2003. Carbon dioxide exchange over agricultural landscape using eddy correlation and footprint modelling. Agric. For. Meteorol. 114, 153–173.
Still, C.J., Berry, J.A., Collatz, G.J., DeFries, R.S., 2003. Global distribution of C3 and C4 vegetation: carbon cycle implications. Global Biogeochem. Cycles 17 (1), 1006, doi:10.1029/2001GB001807.
Tao, F., Yokozawa, M., Zhang, Z., Xu, Y., Hayashi, Y., 2005. Remote sensing of crop production in China by production efficiency models: models comparisons, estimates and uncertainties. Ecol. Model. 183, 385–396.
Turner, D.P., Urbanski, S., Bremer, D., Wofsy, S.C., Meyers, T., Gower, S.T., Gregory, M., 2003. A cross-biome comparison of daily light use efficiency for gross primary production. Global Change Biol. 9, 383–395.
Vina, A., Gitelson, A.A., Rundquist, D.C., Keydan, G., Leavitt, B., Schepers, J., 2004. Remote sensing—monitoring maize (*Zea mays* L.) phenology with remote sensing. Agron. J. 96, 1139–1147.
Webb, E.K., Pearman, G.I., Leuning, R., 1980. Correction of flux measurement for density effects due to heat and water vapour transfer. Q. J. R. Meteorol. Soc. 106, 85–100.
Weiss, A., Norman, J.M., 1985. Partitioning solar-radiation into direct and diffuse, visible and near-infrared components. Agric. For. Meteorol. 34, 205–213.
White, M.A., Thornton, P.E., Running, S.W., 1997. A continental phenology model for monitoring vegetation responses to interannual climatic variability. Global Biogeochem. Cycles 11, 217–234.

Wilczak, J., Oncley, S., Stage, S., 2001. Sonic anemometer tilt correction algorithms. Boundary Layer Meteorol. 99, 127–150.

Wilson, K.B., Baldocchi, D.D., Hanson, P.J., 2001. Leaf age affects the seasonal patterns of photosynthetic capacity and net ecosystem exchange of carbon in a deciduous forest. Plant Cell Environ. 24, 571–583.

Wofsy, S.C., Goulden, M.L., Munger, J.W., Fan, S.M., Bakwin, P.S., Daube, B.C., Bassow, S.L., Bazzaz, F.A., 1993. Net exchange of CO_2 in a mid-latitude forest. Science 260, 1314–1317.

Xiao, X.M., 2006. Light absorption by leaf chlorophyll and maximum light use efficiency. IEEE Trans. Geosci. Remote 44, 1933–1935.

Xiao, X., Boles, S., Frolking, S., Salas, W., Moore, B., Li, C., He, L., Zhao, R., 2002. Observation of flooding and rice transplanting of paddy rice fields at the site to landscape scales in China using VEGETATION sensor data. Int. J. Remote Sens. 23, 3009–3022.

Xiao, X.M., Braswell, B., Zhang, Q.Y., Boles, S., Frolking, S., Moore, B., 2003. Sensitivity of vegetation indices to atmospheric aerosols: continental-scale observations in Northern Asia. Remote Sens. Environ. 84, 385–392.

Xiao, X.M., Hollinger, D., Aber, J., Goltz, M., Davidson, E.A., Zhang, Q.Y., Moore, B., 2004a. Satellite-based modeling of gross primary production in an evergreen needleleaf forest. Remote Sens. Environ. 89, 519–534.

Xiao, X.M., Zhang, Q.Y., Braswell, B., Urbanski, S., Boles, S., Wofsy, S., Moore, B., Ojima, D., 2004b. Modeling gross primary production of temperate deciduous broadleaf forest using satellite images and climate data. Remote Sens. Environ. 91, 256–270.

Xiao, X.M., Zhang, Q.Y., Hollinger, D., Aber, J., Moore, B., 2005a. Modeling gross primary production of an evergreen needleleaf forest using MODIS and climate data. Ecol. Appl. 15, 954–969.

Xiao, X.M., Zhang, Q.Y., Saleska, S., Hutyra, L., De Camargo, P., Wofsy, S., Frolking, S., Boles, S., Keller, M., Moore, B., 2005b. Satellite-based modeling of gross primary production in a seasonally moist tropical evergreen forest. Remote Sens. Environ. 94, 105–122.

Xiao, X.M., Boles, S., Frolking, S., Li, C.S., Babu, J.Y., Salas, W., Moore, B., 2006. Mapping paddy rice agriculture in South and Southeast Asia using multi-temporal MODIS images. Remote Sens. Environ. 100, 95–113.

Xin, J., Yua, Z.R., van Leeuwen, L., Driessen, P.M., 2002. Mapping crop key phenological stages in the North China Plain using NOAA time series images. Int. J. Appl. Earth Obs. Geoinf. 4, 109–117.

Yan, H., Liu, J., Cao, M., 2005. Remotely sensed multiple cropping index variations in China during 1981–2000. Acta Geogr. Sin. 60, 559–566.

Yu, G.R., Fu, Y.L., Sun, X.M., Wen, X.F., Zhang, L.M., 2006. Recent progress and future directions of ChinaFLUX. Sci. China Ser. D Earth Sci. 36, 1–23.

Zhang, X.Y., Friedl, M.A., Schaaf, C.B., Strahler, A.H., Hodges, J.C.F., Gao, F., Reed, B.C., Huete, A., 2003. Monitoring vegetation phenology using MODIS. Remote Sens. Environ. 84, 471–475.

Zhang, X.Y., Friedl, M.A., Schaaf, C.B., 2006. Global vegetation phenology from moderate resolution imaging spectroradiometer (MODIS): evaluation of global patterns and comparison with in situ measurements. J. Geophys. Res. Biogeogr. 111.

Zhang, Y., Yu, Q., Jiang, J.I.E., Tang, Y., 2008. Calibration of Terra/MODIS gross primary production over an irrigated cropland on the North China Plain and an alpine meadow on the Tibetan Plateau. Global Change Biol. 14, 757–767.

Zhao, F.H., Yu, G.R., Li, S.G., Ren, C.Y., Sun, X.M., Mi, N., Li, J., Ouyang, Z., 2007. Canopy water use efficiency of winter wheat in the North China Plain. Agric. Water Manage. 93, 99–108.